Q. J. R. Meteorol. Soc. (1994), **120**, pp. 699–712 551.513.1:551.511.31:551.510.52(215–17)

The northern hemisphere tropospheric response to changes in the gravity-wave drag scheme in a perpetual January GCM

By DAVID B. STEPHENSON*
University of Reading, UK

(Received 4 January 1993; revised 11 October 1993)

SUMMARY

The sensitivity of a general-circulation-model climatology to changes in the gravity-wave drag scheme is investigated with particular emphasis being placed upon the northern hemisphere wintertime tropospheric circulation. It is found that by weakening the upper-level drag, the Ferrel-cell circulation intensifies to the north, resulting in a greater than 10 K cooling in the region of the arctic tropopause. The poleward side of the northern hemisphere sub-tropical jet intensifies in the region of 60–70°N, and a poleward shift is observed in the eddy meridional momentum flux. A large part of the response is zonally asymmetric, with the Aleutian and Icelandic lows becoming shallower with weakened upper-level gravity-wave drag. By comparing the results of a gravity-wave drag scheme having a wave-breaking vertical profile with those of a simple uniform drag-profile scheme it appears that the tropospheric response to weakened upper-level drag depends very little upon the choice of vertical drag profile in the troposphere.

1. INTRODUCTION

Orographic gravity-wave drag (GWD) schemes were first introduced into general circulation models (GCMs) by Boer *et al.* (1984) and McFarlane (1987) in order to reduce the excessive westerlies found in the northern hemisphere mid latitudes in high horizontal resolution models. GWD schemes crudely model the increased drag on the atmosphere above mountains that is caused by vertically propagating and breaking internal gravity waves too small to be explicitly resolved by the GCM. From the few observations available, it is believed that the induced drag occurs mainly in a few kilometres above the mountains and at around 10–100 mb in the lower stratosphere.

A GWD scheme was proposed and introduced into the UK Meteorological Office atmosphere model in 1986 by Palmer *et al.* (1986) who showed that, as well as reducing the excessive westerlies, it had the benefit of diminishing the excessive cold bias in the arctic upper troposphere and lower stratosphere. They demonstrated that the stratospheric drag in mid latitudes forced a direct meridional circulation that brought air northwards and downwards into the arctic upper troposphere which warmed adiabatically. The same scheme was introduced into the European Centre for Medium-range Weather Forecasts (ECMWF) forecast model in 1986 and it gave reduced systematic errors in the global angular momentum budget and improved forecast skills (Miller *et al.* 1989).

However, longer integrations of 90 days by Miller (1986) revealed that the amount of drag in the upper levels was excessive. This was confirmed by the detailed momentum-budget study performed by Klinker and Sardeshmukh (1992). To alleviate the problem a new GWD scheme was introduced into the ECMWF model in 1989 (Miller and Palmer 1989) with two major differences to that of the 1986 scheme. Firstly, and most importantly, the new scheme had an altered vertical profile for the stress distribution, giving more deceleration below 800 mb and less above 100 mb than in the 1986 scheme. Secondly, an additional gravity-wave stress was included at all grid points whenever the low-level inverse Froude number exceeded a prescribed value. This high inverse Froude-number stress was added in order to account for the effects of nonlinear gravity-wave resonance, low-level trapping, and enhanced low-level drag due to upstream damming.

*Present address: Météo-France, 42 Ave. G. Coriolis, Toulouse 31057 Cedex, France.

Because of the large impact of GWD schemes on northern hemisphere wintertime climatology in atmosphere models, it is important to perform sensitivity studies of GWD schemes in GCMs. Examples of features that have received little attention are the transient and stationary eddies. Using a GCM derived from the 1987 ECMWF forecast model, this study attempts to understand better the response caused by changing from the 1986 to the 1989 GWD scheme.

2. The experimental procedure

(*a*) *The model*

The GCM used in these studies is the UK Universities Global Atmospheric Modelling Programme (UGAMP) model which was derived from the 1987 cycle 27 ECMWF spectral forecast model described by Tiedtke *et al.* (1988) and Palmer *et al.* (1990). The model has a Morcrette radiation scheme (Morcrette 1990) and a Kuo convection scheme (Kuo 1974). Sea surface temperatures are prescribed from climatology. It has been found that a truncation of T42 and 19 vertical levels gives results in reasonable agreement with northern hemisphere wintertime observations, whereas at lower resolutions, such as T21, the transient features in the northern hemisphere stormtracks are poorly simulated. For a description of the model's performance in simulating the analysed northern-winter climatology refer to Boer *et al.* (1991).

(*b*) *The gravity-wave drag scheme*

In the ECMWF model the zonal wind tendency due to GWD can be written as:

$$\frac{\partial \mathbf{u}}{\partial t} = -g\frac{\partial \tau}{\partial p} \tag{1}$$

with the GWD stress at pressure level, p, given by $\tau(\lambda, \theta, p) = \tau^0(\lambda, \theta)f(p)$ where (λ, θ) are the longitude and latitude coordinates respectively.

In the 1986 ECMWF scheme the surface stress, τ^0, is calculated, using knowledge of the low-level inverse Froude number $Fr = N_L h/U_L$, by the expression,

$$\tau^0 = \kappa\rho_L \mathbf{U}_L U_L^2 N_L^{-1}\,\mathrm{Min}(Fr_L^2, Fr_c^2) \tag{2}$$

where subscript L refers to the low-level flow (defined by the ECMWF as the mass-weighted lowest three model levels). The height, h, is the sub-grid-scale standard deviation of the orography in the direction of the quadrant in which the low-level wind $\mathbf{U}_L$ points. The critical inverse Froude number, Fr_c, is set to the value of 2. The above definition has the property that τ^0 varies as the cube of U_L for small U_L, and varies linearly with U_L for larger values where $Fr < Fr_c$.

In the 1989 scheme there is an additional high inverse-Froude-number stress given by

$$\tau^0 = \begin{cases} 0 & Fr < Fr_c \\ \kappa_s\rho_L \mathbf{U}_L U_L^2 N_L^{-1}\,(Fr - Fr_c)^2\, G(\lambda, \theta) & Fr \geq Fr_c \end{cases} \tag{3}$$

where $G(\lambda, \theta)$ attempts to describe the isotropy of the sub-grid-scale variances, and ranges from zero for 1-dimensional orography (e.g. a long mountain ridge) to unity for more isotropic orography. None of the experiments in this paper include this additional stress; preliminary experiments revealed that its inclusion caused only a small impact on the large-scale general circulation.

In the 1986 scheme the vertical profile of stress is calculated using a saturation hypothesis based upon a wave Richardson-number criterion i.e. $f(p) = f_w(p)$. The stress diminishes monotonically with height from τ^0 at the ground to zero at the top of the model owing to dissipation caused by breaking gravity waves. Gravity-wave breaking for a zero phase speed gravity wave occurs in the region of critical heights where the wind is zero. The 1986 scheme can be generalized to give uniform drag for levels below $p = p'$, as follows:

$$f(p) = \begin{cases} \beta + (1-\beta)(p-p')(p^0-p')^{-1} & p \geq p' \\ \beta f_w(p) & p < p' \end{cases} \tag{4}$$

where p^0 is the surface pressure. The 1986 scheme is obtained by setting $\beta = 1$ and $p' > p^0$. The 1989 scheme uses values of $\beta = 0.3$ and $p' = 800$ mb, having the net effect of depositing less drag at upper-levels and more drag at lower levels below 800 mb. Uniform drag for all heights can be obtained by setting $\beta = 0$ and $p' = 0$ and, in this case, there is no description made of the enhanced drag caused by gravity waves breaking at critical levels.

(c) *The experiments*

Three 120-day experiments were performed with the UGAMP model at 19-level T42 resolution, having solar insolation and sea surface temperatures fixed at January mean values. The first 60 days of the runs were used for spin-up and the remaining 60 days were used for obtaining the time-mean results. Given the large amount of low-frequency variability in the stormtrack regions, it might appear that 60 days is too short a period to obtain a statistically significant signal between the experiments. However, the results show large sensitivity to changes in the GWD scheme, and hence it is believed that the signal is large enough to be seen above the variability even in such short climate runs. This hypothesis is supported by the large spatial coherence seen in the results and in the way in which the qualitative response to weakened drag is seen to agree with the theory presented in Palmer *et al.* (1986).

The control experiment, STRGWD, was performed using the 1986 ECMWF GWD scheme which has STRong drag in the upper levels. Two additional experiments were performed having different vertical stress profiles with less upper-level drag than that of the control experiment. WEAGWD used the 1989 ECMWF GWD scheme, with the exception of the additional high inverse-Froude-number stress, which is currently operational at ECMWF, and uses $\beta = 0.3$ and $p' = 800$ mb to give less drag at upper levels and more drag at lower levels. The third experiment, LINGWD, had a vertical stress distribution which was solely LINear with pressure from the surface to the top of the model ($\beta = 0$ and $p' = 0$). Such a simplistic definition is flow-independent and takes no account of critical-layer effects. Comparison of such a simplified scheme with the other more realistic schemes allows one to assess the importance of including flow-dependence and critical-line absorption in GWD schemes. All three experiments have the same formulation for the surface stress and differ only in the vertical distribution of the stress.

Figure 1 shows the time-mean northern hemisphere distribution of the zonal component of the surface stress for the three experiments. It can be seen that all three experiments give similar values. Changes in the low-level flow, caused by having differing vertical stress distributions, appear to have only a small effect on the time-mean low-level stress, as evidenced by the similarity of the three figures. Figure 2 shows the time-mean zonal-wind tendency zonally averaged over land areas for the three experiments. In STRGWD the deceleration reaches values of 8 m s^{-1} day^{-1} at 50 mb and below 800 mb. In WEAGWD the upper-level deceleration at 50 mb is less than about 2 m s^{-1} day^{-1},

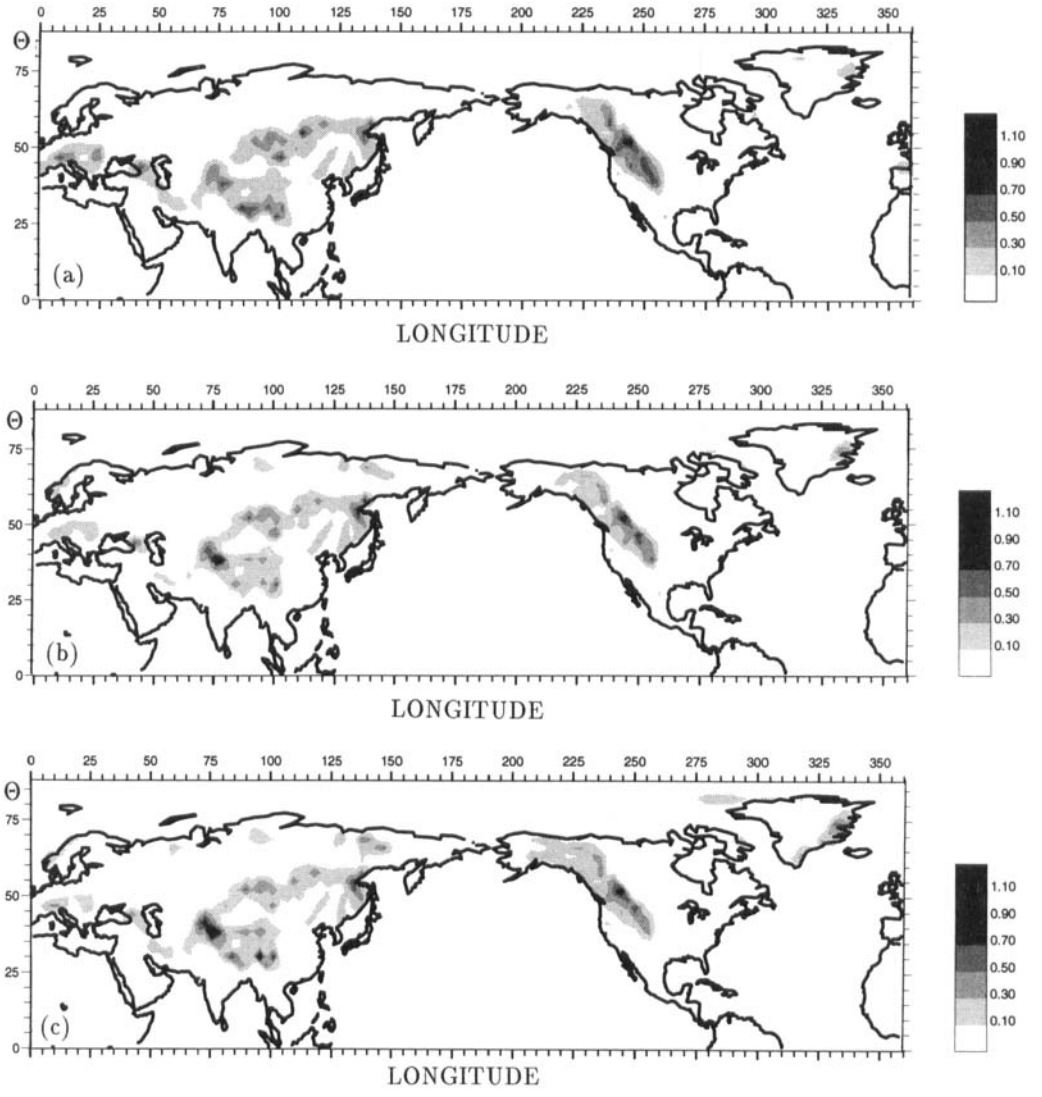

Figure 1. Time-mean zonal component of the gravity-wave drag surface stress for the experiments (a) STRGWD (b) WEAGWD and (c) LINGWD. Units are in $N\,m^{-2}$.

and hence is much weaker than in STRGWD. The deceleration below 800 mb in WEAGWD is dominated by the uniform drag profile and reaches maximum values of $7\,m\,s^{-1}\,day^{-1}$. In LINGWD the deceleration is uniform with pressure, as expected, and has maximum values of $1.5\,m\,s^{-1}\,day^{-1}$, and hence has upper-level tendencies similar to those exhibited in WEAGWD.

3. The results

As stated earlier, the STRGWD experiment is treated as the control experiment and so the responses caused by having weaker upper-level drag, WEAGWD − STRGWD and LINGWD − STRGWD, will be presented.

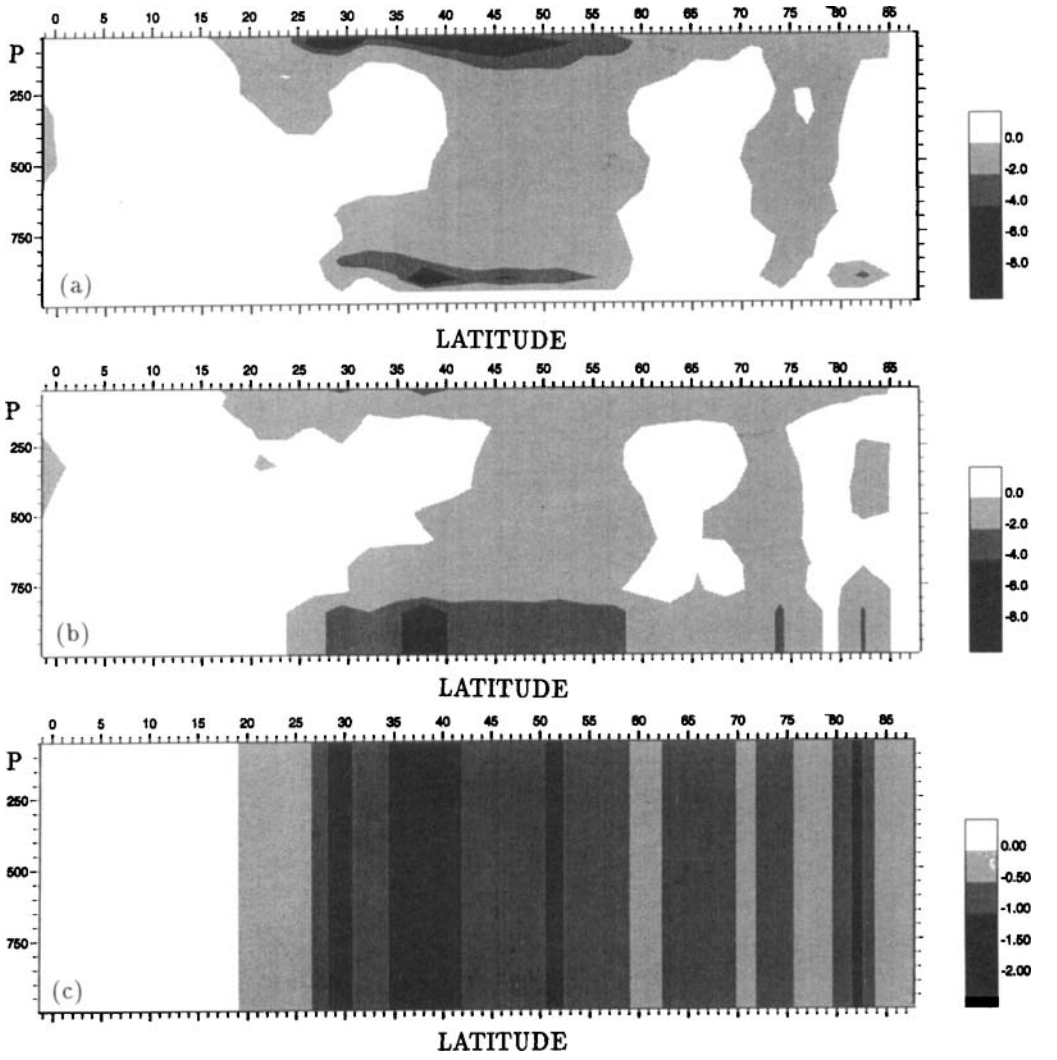

Figure 2. Time-mean zonal wind tendency, zonally averaged over land, due to gravity-wave drag for the experiments (a) STRGWD (b) WEAGWD and (c) LINGWD. Units are in $m\,s^{-1}\,day^{-1}$ and are negative. Note the differing scale in (c).

(*a*) *Zonal-mean zonal wind response*

Figure 3, shows the northern hemisphere zonal-mean zonal wind responses superimposed on the westerly mean zonal wind contours of the control experiment. It can be seen that both WEAGWD and LINGWD give a similar response, consisting of an equatorward weakening and a poleward strengthening of the zonal wind. The response is strongest above 200 mb, and represents a poleward shift of the polar-night jet. Below 200 mb the response is of the order of 5–10 $m\,s^{-1}$ and is centred upon higher latitudes than the upper-level response. With weaker drag the westerlies at 60–70°N strengthen on the poleward side of the sub-tropical jet, which brings them into closer agreement with those in the analysed climatology presented by Hoskins *et al.* (1989, p. 73). It is of interest to compare Fig. 3 with Fig. 15(a) in Palmer *et al.* (1986) which shows the

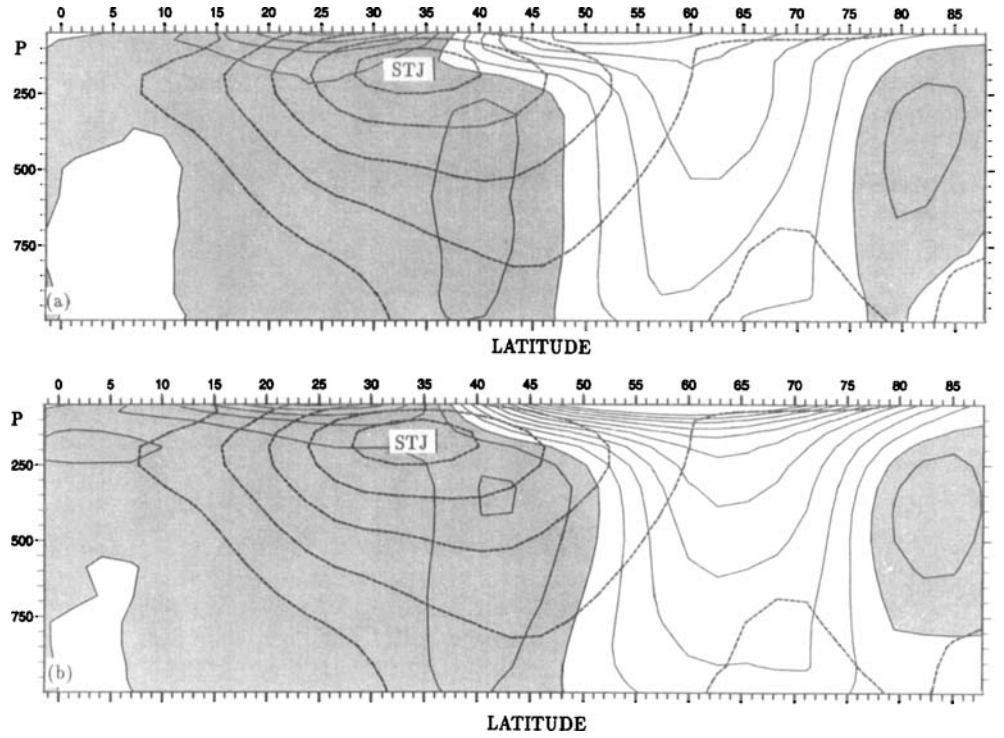

Figure 3. Time-mean zonal-mean zonal wind response of (a) WEAGWD − STRGWD and (b) LINGWD − STRGWD. The contour interval is 2 m s^{-1} and negative values are shaded. The dashed lines are the 10 m s^{-1} contours of the time-mean zonal-mean westerly zonal wind in STRGWD and demark the position of the sub-tropical jet.

difference in the zonal-mean zonal wind between a model with the 1986 GWD scheme and one with no GWD scheme; the response in Fig. 3 is almost the opposite to that shown there. Hence, as might be expected, the weaker drag runs are behaving somewhere in between the extreme cases of having a lot of upper-level drag (the 1986 GWD scheme) and the case of having no GWD.

(*b*) *Thermal and meridional circulation response*

Figure 4 shows the northern hemisphere temperature and mean meridional circulation (MMC) responses. Both the WEAGWD and LINGWD experiments show similar responses, having an induced indirect circulation centred at 55°N, resulting from a strengthened Ferrel-cell circulation to the north in the weaker drag cases, and an order 10 K cooling of the upper arctic troposphere. The induced indirect circulation and the associated adiabatic coolings are in agreement with the idea that the weaker drag response is the negative of the drag minus no-drag response shown in Palmer *et al.* (1986).

(*c*) *Zonal-mean zonal momentum analysis*

In this section the budget of the time-mean zonal-mean zonal wind equation will be presented as an aid to understanding the response to the different GWD schemes.

For long period time-averages, the zonal-mean of the zonal-wind-tendency primitive equation on pressure surfaces can be written as the sum of the MMC and eddy terms balancing the total forcing term:

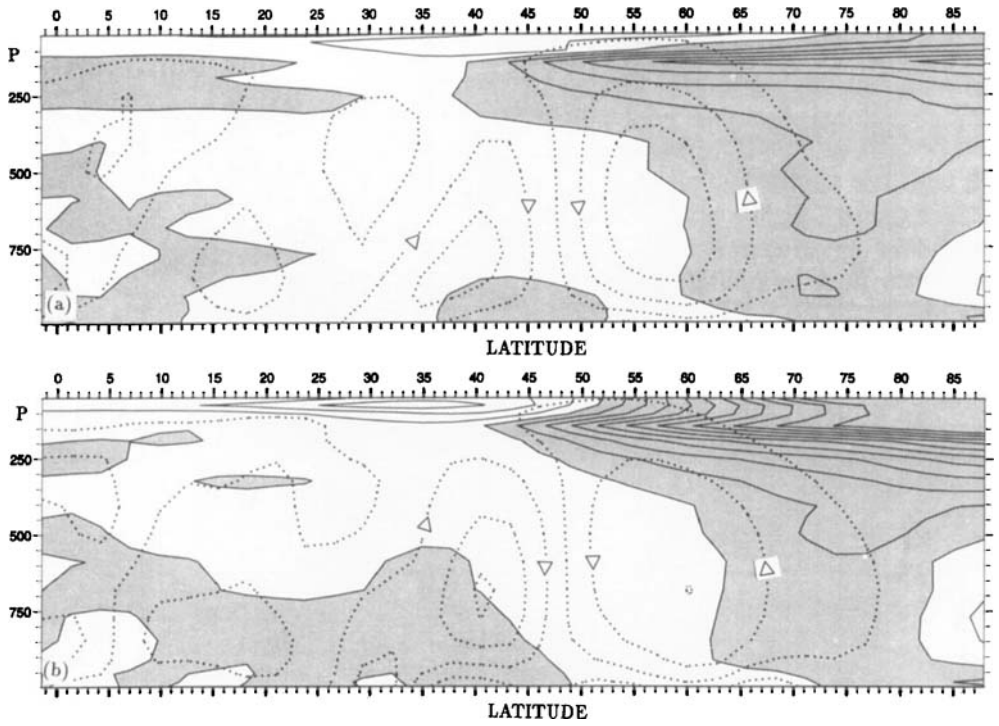

Figure 4. Temperature (solid line) and mean meridional circulation stream-function (dotted line) response of (a) WEAGWD − STRGWD and (b) LINGWD − STRGWD. The temperature contour interval is 2 K and negative values are shaded. The stream-function contour interval is 10^{10} K g s^{-1}.

$$(-f[\overline{v}] + D_y([\overline{u}][\overline{v}]) + \partial_p([\overline{u}][\overline{w}])) + (D_y[\overline{u^*v^*}] + \partial_p[\overline{u^*w^*}]) = [\overline{F_x}] \tag{5}$$

where $[X]$ denotes the zonal-mean, X^* denotes the deviation from the zonal-mean (i.e. eddy) and $\overline{X}$ denotes the time-mean of the quantity X. The meridional derivative, D_y, is defined as:

$$D_y X = \frac{1}{a\cos^2\theta}\frac{\partial}{\partial\theta}(X\cos^2\theta) \tag{6}$$

where a is the earth's radius. The total mechanical forcing, F_x, is the result of GWD, $-g\partial_p\tau$, boundary-layer drag, and vertical and horizontal diffusion in the model.

The sum of the MMC and eddy terms is presented for the climatology of STRGWD in Fig. 5(a), and for the response, WEAGWD − STRGWD, in Fig. 5(b). The results of LINGWD − STRGWD were found to be very similar to those of WEAGWD − STRGWD and will not be presented for the sake of brevity. In Fig. 5(a) large values, exceeding 10 m s^{-1} day^{-1}, occur below 750 mb as a result of strong surface drag; the sign changes depending upon whether the mean zonal wind is easterly or westerly. An upper-level maximum of about 3 m s^{-1}day^{-1} can also be seen centred upon 45°N and 50 mb and is a consequence of the upper-level maximum seen in the orographic GWD in Fig. 2(a). The MMC and eddy parts of the total in Fig. 5(a) are shown in Fig. 6, where it can be seen that there is large cancellation between the two parts in the free atmosphere. The total below 750 mb comes mainly from the MMC term whilst the GWD maximum at upper levels is the residual term of the large MMC and eddy terms.

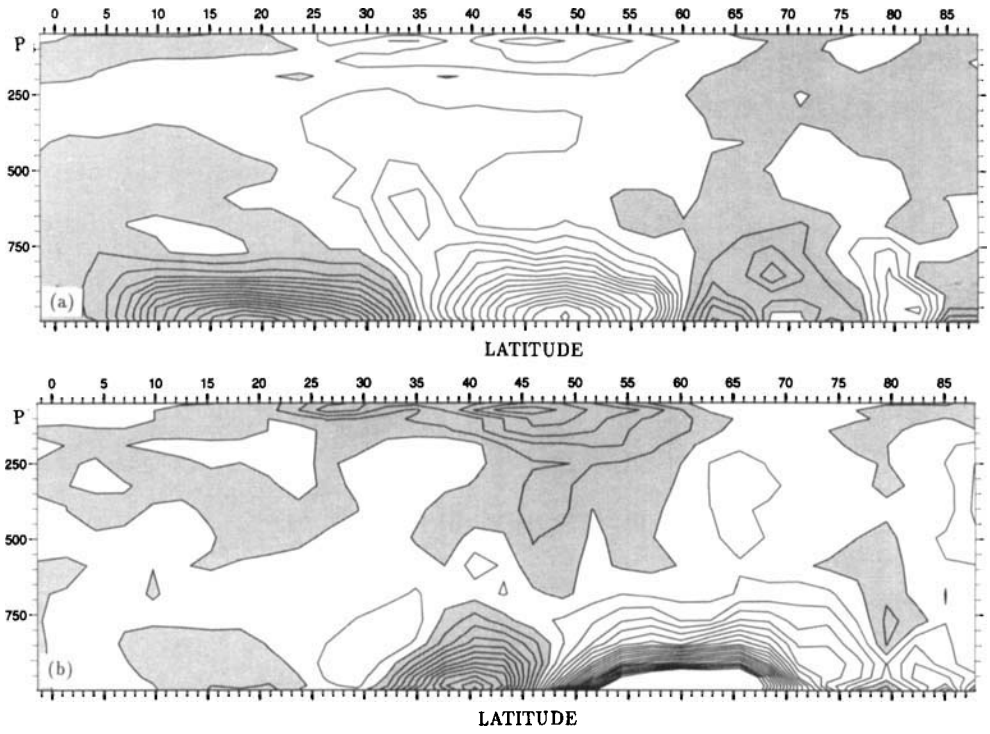

Figure 5. The sum of the mean meridional circulation and eddy parts of the zonal momentum budget for (a) STRGWD (contour interval of 1 m s^{-1} day^{-1}) and (b) WEAGWD − STRGWD (contour interval of 0.5 m s^{-1} day^{-1}). Negative values are shaded.

The WEAGWD − STRGWD response shown in Fig. 5(b) has values of the order of 5–10 m s^{-1} day^{-1}. Below 750 mb a dipole pattern can be seen centred on 45°N, with increased drag to the north and decreased drag to the south consistent with the poleward strengthening of the zonal wind previously discussed. At upper levels there is a decrease by about 3 m s^{-1} day^{-1}, as to be expected from the weakened GWD at upper levels shown in Fig. 2. Figure 7 shows the MMC and the Coriolis-term contributions to the response shown in Fig. 5(b). The similarity of Fig. 7(a) and Fig. 7(b) shows that a large part of the MMC response is described by changes in $f[\overline{v}]$ related to changes in the Ferrel-cell circulation. Below 750 mb the poleward strengthening of the Ferrel cell balances almost completely the increased low-level drag north of 45°N.

Figure 8 shows the eddy momentum flux contributions to the response. The similarity of Fig. 8(a) and Fig. 8(b) indicates that the dominant role is played by the meridional convergence of the poleward eddy momentum flux, i.e. $-D_y[\overline{u^*v^*}]$. Comparing Fig. 8(b) with Fig. 7(b) it can be seen that there is large cancellation between the two terms and that the response of each term is greater than the response of the sum, and is not localized to the region where the GWD has changed. The meridional convergence of the poleward momentum flux shows a very clear tripolar signature at upper levels with acceleration around 33°N and 60°N and deceleration at 45°N. As discussed by Pfeffer (1987), the horizontal convergence of poleward momentum correlates well with the zonal momentum tendency in mid latitudes, indicating that the increased zonal wind at 60°N seen in the

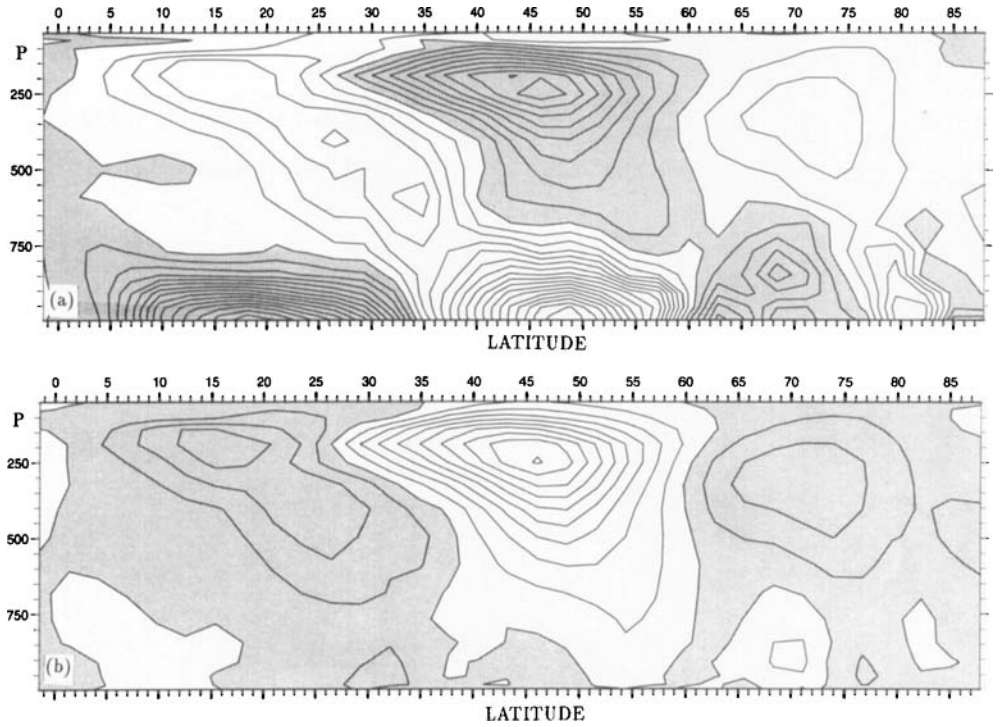

Figure 6. The components of the zonal-mean zonal momentum budget for STRGWD; (a) mean meridional circulation component and (b) eddy component. The contour interval is 1 $m s^{-1}$ day^{-1}. Negative values are shaded.

responses may be caused by the increased convergence of eddy momentum flux at these latitudes.

The results have shown that the change in the drag leads to large opposite responses in the MMC and eddy terms, leaving the total response as a small residual term. The possibility that a transformed Eulerian-mean diagnosis would obviate this problem was investigated by examining the response of the residual MMC and the Eliassen–Palm (EP) divergence following Edmon *et al.* (1980). In agreement with the results of Pfeffer (1987), a large part of the EP divergence response, due to the vertical divergence of heat fluxes, was found to be cancelled by the residual MMC response, thus giving the total forcing as a small residual term once again.

The response of the poleward eddy momentum fluxes are shown for both the WEAGWD and LINGWD experiments in Fig. 9. The response consists of a poleward shift of the fluxes together with a weakening of the meridional gradient. More than 50% of the change is accounted for by changes in the eddy momentum flux due to transient eddies. Figure 10 shows the zonally averaged meridional momentum flux due to all the transients $[\overline{u'v'}]$ for the STRGWD and WEAGWD experiments; the LINGWD results look almost identical to the WEAGWD ones and so have not been presented. There is a large difference in the northern hemisphere between the two experiments; this suggests that upper-level GWD can have a significant effect on the horizontal phase tilt of tropospheric transient eddies in the northern hemisphere. In the southern hemisphere

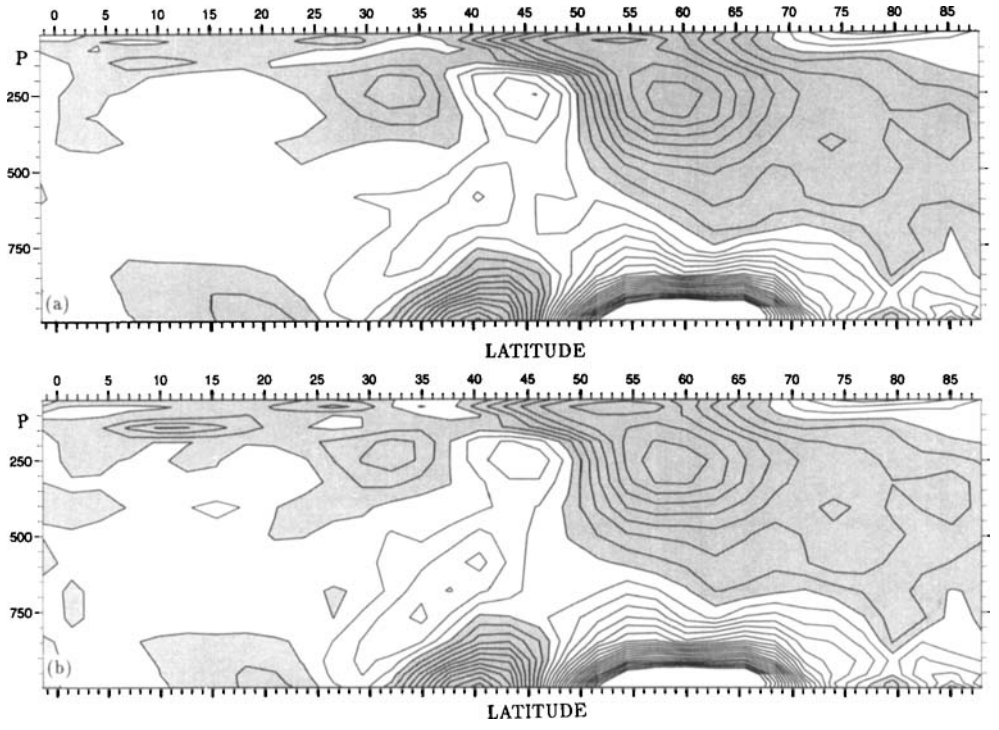

Figure 7. The components of the zonal-mean zonal momentum budget for WEAGWD – STRGWD; (a) mean meridional circulation component and (b) $-f[\overline{v}]$ component. The contour interval is $0.5\,\mathrm{m\,s^{-1}\,day^{-1}}$. Negative values are shaded.

where GWD is expected to play a lesser role, there is only a small difference in the transient fluxes. Compared with analysed wintertime transient eddy momentum fluxes, Hoskins *et al.* (1989, p. 74), the STRGWD results have a much too deep minimum north of 50°N, which is improved in the WEAGWD results. However, the maximum in the analysed results is about $40\,\mathrm{m^2\,s^{-2}}$ compared with about $60\,\mathrm{m^2\,s^{-2}}$ seen in the GCM results; this is probably related to deficiencies in other parametrizations, such as in the horizontal-diffusion scheme.

(*d*) *The upper-level stationary-wave response*

Zonal-mean results have been presented and little has been said of the zonally asymmetric response to changes in the GWD scheme. Figure 11 shows the WEAGWD and LINGWD responses of the time-mean eddy part of the 200 mb stream function. Compared with typical stationary-wave values of $30 \times 10^6\,\mathrm{m^2\,s^{-1}}$, the changes are large. The response is yet again similar in both the WEAGWD and LINGWD experiments and has largest magnitudes over North America and the North Atlantic. The low-high-low-high pattern extending from the coast of California to the Saharan coast of Africa is possibly a stationary Rossby wave-train response, propagating in the region of the strong westerlies.

Two highs exist in the upper-level response at around latitude 45°N and longitudes 160°W and 10°W, and these are the predominant features which appear as 10 mb highs

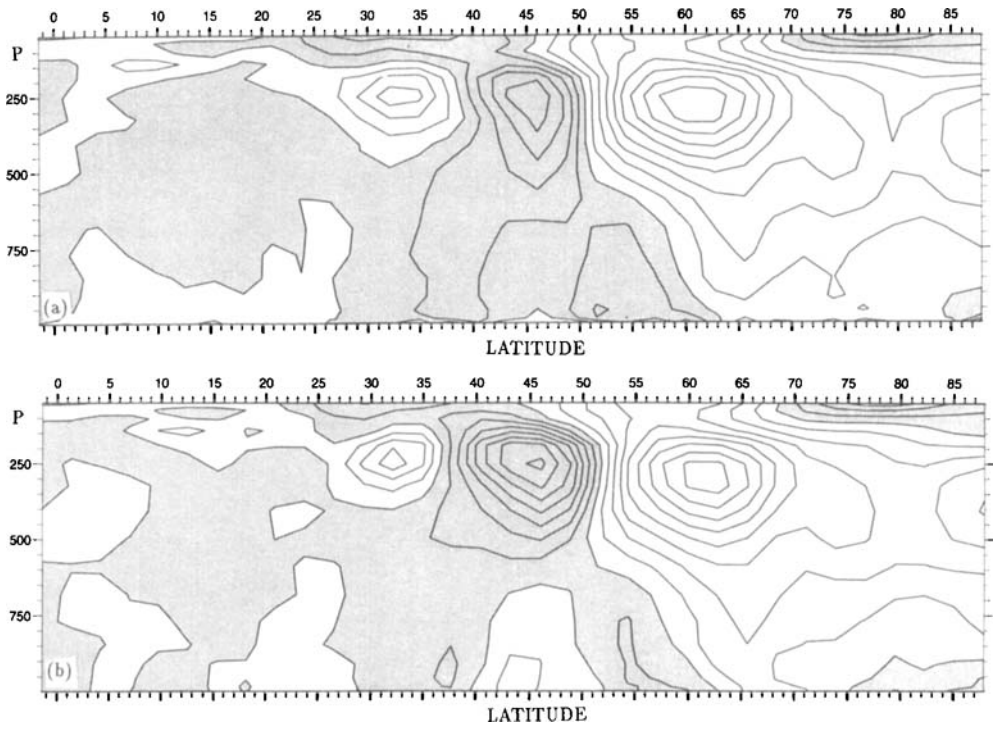

Figure 8. The components of the zonal-mean zonal momentum budget for WEAGWD − STRGWD; (a) total eddy component and (b) $D_y\overline{[u^*v^*]}$ component. The contour interval is $0.5\,m\,s^{-1}\,day^{-1}$. Negative values are shaded.

in the sea-level pressure response and the surface winds; with weaker upper-level GWD the Aleutian and Icelandic lows are not as deep and the flow is more zonal, as pointed out in Palmer *et al.* (1986).

4. Concluding remarks

It has been shown from the results of 120-day GCM integrations that changing the GWD scheme from the 1986 ECMWF GWD scheme to the 1989 ECMWF GWD scheme results in a large change in the northern hemisphere wintertime climatology. The zonal-mean response shows an intensification of about $5–10\,m\,s^{-1}$ to the north of the sub-tropical jet, a strengthening of the Ferrel cell around 60°N, and a cooling of 10 K near the arctic tropopause. All the results are in agreement with the arguments presented in Palmer *et al.* (1986) for the effect caused by upper-level drag on the tropospheric–stratospheric circulation by the creation of a direct meridional circulation which causes air to warm adiabatically as it descends into the arctic troposphere.

In addition, a large increase of around $50\,m^2\,s^{-2}$ occurs in the eddy meridional momentum flux centred on 55°N and 200 mb. More than 50% of this is caused by changes in the transient eddy meridional momentum flux and suggests that the horizontal phase tilt of the mature baroclinic waves at the ends of the stormtrack are strongly dependent

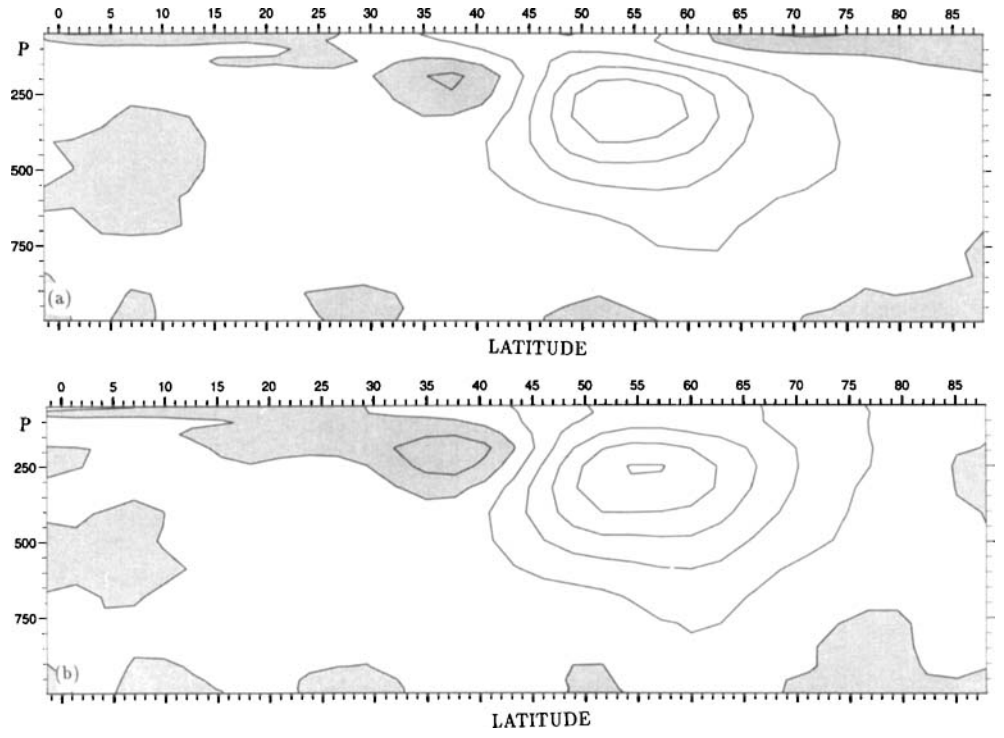

Figure 9. Eddy meridional momentum flux $\overline{[u^*v^*]}$ response of (a) WEAGWD − STRGWD and (b) LINGWD − STRGWD. The contour interval is $10\,m^2s^{-2}$ and negative values are shaded.

on upper-level drag due to orographic gravity waves. It may be that the reduced cyclonic shear on the poleward side of the sub-tropical jet in the weaker GWD case is causing the more northern transients to roll up less cyclonically, thus reducing the magnitude of the equatorward momentum flux centred at 60°N (Thorncroft *et al.* 1993).

For all the examined fields, both WEAGWD and LINGWD gave similar results even though there is a large difference in their vertical GWD profiles. This suggests that the tropospheric climatology is not sensitive to the vertical drag profile in the troposphere, but is mainly dependent on the amount of drag in the stratosphere. This example of a downward control principle (Haynes *et al.* 1991) indicates that it may be possible to simplify the GWD schemes used in GCMs with no ensuing loss in accuracy.

Acknowledgements

The motivation to perform an experiment with a uniform drag profile was provided during conversations with Professor Brian Hoskins. I also wish to thank Martin Miller for providing me with useful ECMWF internal reports and for enlightening discussions. The GCM runs and analysis were only made possible by the kind assistance of M. Blackburn, J. Slingo, L. Steenman-Clark and J. Thuburn. Appreciation also goes to Martin Juckes for the use of his powerful graphics program.

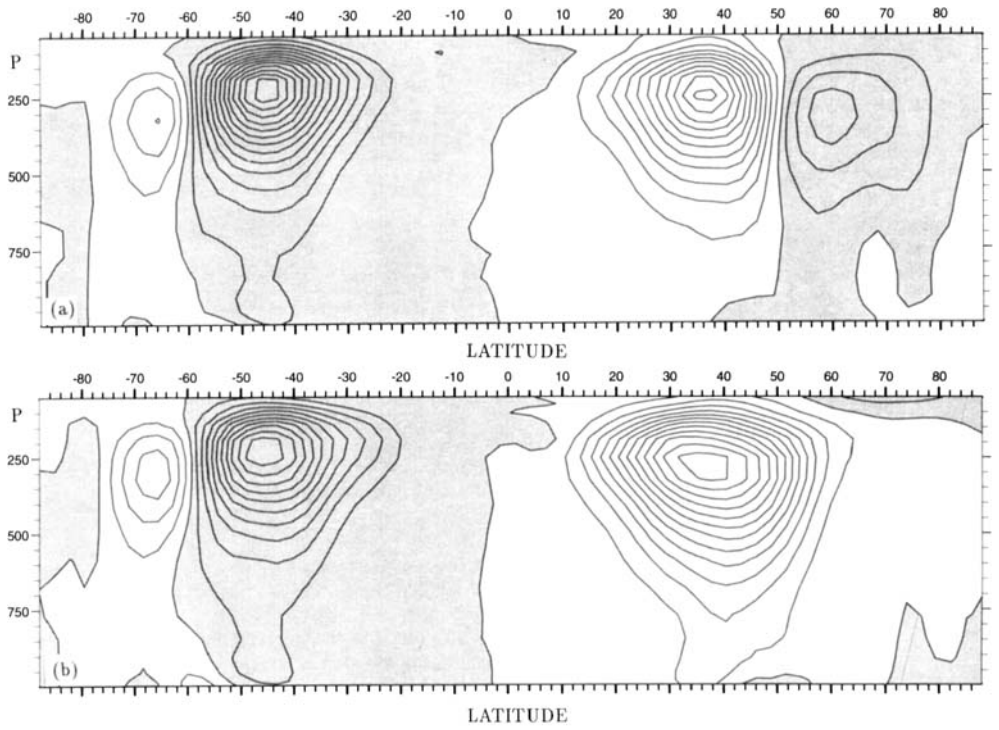

Figure 10. Transient meridional momentum flux $\overline{[u'v']}$ in the experiments (a) STRGWD and (b) WEAGWD. The contour interval is 5 $m^2 s^{-2}$ and negative values are shaded.

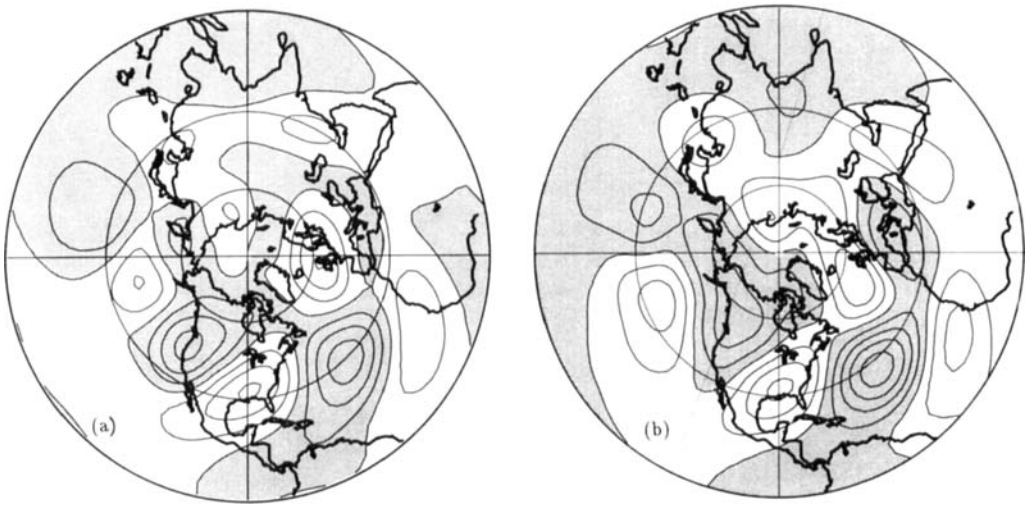

Figure 11. Eddy part of the 200 mb time-mean stream-function response for (a) WEAGWD − STRGWD and (b) LINGWD − STRGWD. The contour interval is 5 × 10^6 $m^2 s^{-1}$ and negative values are shaded.

References

Boer, G. J., McFarlane, N. A., Laprise, R., Henderson, J. D. and Blanchet, J.-P. 1984 The Canadian Climate Centre spectral atmospheric general circulation model. *Atmos.-Ocean*, **22**, 397–429

Boer, G. J., Arpe, K., Blackburn, M., Déqué, M., Gates, W. L., Hart, T. L., le Treut, H., Roeckner, E., Sheinin, D. A., Simmonds, I., Smith, R. N. B., Tokioka, T., Wetherald, R. T. and Williamson, D. 1991 An intercomparison of the climates simulated by 14 atmospheric GCMs. CAS/JSC-15, WMO/TD-No. 425

Edmon, H. J., Hoskins, B. J. and McIntyre, M. E. 1980 Eliassen–Palm cross sections for the troposphere. *J. Atmos. Sci.*, **37**, 2600–2616

Haynes, P. H., Marks, C. J., McIntyre, M. E., Shepherd, T. G. and Shine, K. P. 1991 On the downward control of extratropical diabatic circulations by eddy-induced mean zonal forces. *J. Atmos. Sci.*, **48**, 651–678

Hoskins, B. J., Hsu, H. H., James, I. N., Masutani, M., Sardeshmukh, P. D. and White, G. H. 1989 Diagnostics of the global atmospheric circulation. WCRP-27, WMO/TD-No. 326

Klinker E. and Sardeshmukh, P. D. 1992 The diagnosis of mechanical dissipation in the atmosphere from large-scale balance requirements. *J. Atmos. Sci.*, **49**, 608–627

Kuo, H. L. 1974 Further studies of the parameterization of the influence of cumulus convection on large-scale flow. *J. Atmos. Sci.*, **31**, 1232–1240

McFarlane, N. A. 1987 The effect of orographically excited gravity wave drag on the general circulation of the lower stratosphere and troposphere. *J. Atmos. Sci.*, **44**, 1775–1800

Miller, M. J. 1986 'Orographic gravity wave drag'. ECMWF Research Memorandum R2327/1798

Miller, M. J. and Palmer, T. N. 1989 'Proposed revision and enhancement of the gravity wave drag parameterisation scheme'. ECMWF Research Memorandum R2327/2421

Miller, M. J., Palmer, T. N. and Swinbank, R. 1989 Parameterisation and influence of sub-grid scale orography in general circulation and numerical weather prediction models. *Meteorol. Atmos. Phys.*, **40**, 84–109

Morcrette, J.-J. 1990 Impact of changes to the radiation transfer parametrizations plus cloud optical properties in the ECMWF model. *Mon. Weather Rev.*, **118**, 847–873

Palmer, T. N., Shutts, G. J. and Swinbank, R. 1986 Alleviation of systematic westerly bias in general circulation and numerical weather prediction models through an orographic gravity wave drag parametrization. *Q. J. R. Meteorol. Soc.*, **112**, 1001–1039

Palmer, T. N., Branković, C., Molteni, F. and Tibaldi, S. 1990 Extended range predictions with ECMWF models: Interannual variability in operational model integrations. *Q. J. R. Meteorol. Soc.*, **116**, 799–834

Pfeffer, R. L. 1987 Comparison of conventional and transformed Eulerian diagnostics in the troposphere. *Q. J. R. Meteorol. Soc.*, **113**, 237–254

Thorncroft, C. D., Hoskins, B. J. and McIntyre, M. E. 1993 Two paradigms of baroclinic-wave life-cycle behaviour. *Q. J. R. Meteorol. Soc.*, **119**, 17–55

Tiedtke, M., Heckley, W. A. and Slingo, J. 1988 Tropical forecasting at ECMWF: On the influences of physical parametrization on the mean structure of forecasts and analyses. *Q. J. R. Meteorol. Soc.*, **114**, 639–664